NEUROSCIENCE

Hippocampal ripples down-regulate synapses

Hiroaki Norimoto,[1,2] Kenichi Makino,[1*] Mengxuan Gao,[1*] Yu Shikano,[1] Kazuki Okamoto,[1] Tomoe Ishikawa,[1] Takuya Sasaki,[1] Hiroyuki Hioki,[3,4] Shigeyoshi Fujisawa,[2†] Yuji Ikegaya[1,5†]

The specific effects of sleep on synaptic plasticity remain unclear. We report that mouse hippocampal sharp-wave ripple oscillations serve as intrinsic events that trigger long-lasting synaptic depression. Silencing of sharp-wave ripples during slow-wave states prevented the spontaneous down-regulation of net synaptic weights and impaired the learning of new memories. The synaptic down-regulation was dependent on the *N*-methyl-D-aspartate receptor and selective for a specific input pathway. Thus, our findings are consistent with the role of slow-wave states in refining memory engrams by reducing recent memory-irrelevant neuronal activity and suggest a previously unrecognized function for sharp-wave ripples.

Hippocampal and neocortical plasticity during the awake state is dominated by net synaptic potentiation, whereas plasticity during sleep, especially during slow-wave (SW) sleep, is dominated by net synaptic depression (*1*, *2*). These circadian alternations in synaptic weights manifest a homeostatic balancing function for sleep (*3*, *4*); however, the mechanisms behind the synaptic downscaling during SW states remain to be identified. During SW states—which include SW sleep, awake immobility, and consummatory behavior—the hippocampus spontaneously emits transient high-frequency field oscillations called sharp-wave ripples (SWRs) (fig. S1). SWRs represent the reactivation of neurons involved in recently acquired memory (*5*) and contribute to memory consolidation (*6*–*9*). Although memory consolidation may rely on synaptic plasticity, no consensus has yet been reached on the relationship between SWRs and synaptic plasticity (*10*–*12*).

We first investigated whether suppression of SWRs affects the synaptic down-regulation that occurs during SW states. We allowed mice to explore novel environments for 30 min before sleep because SWRs are known to occur more frequently after spatial learning (*13*). Indeed, the 30-min exploration increased the SWR event frequencies from 0.48 ± 0.03 Hz under naïve conditions to 0.88 ± 0.07 Hz (mean ± SEM of eight trials from three mice; $P = 3.1 \times 10^{-8}$, $t_7 = 6.56$, paired *t* test). The SWR increase may reflect the strengthening of synaptic weights in the learning process (*14*). We then perturbed the SWRs during SW states for 7 hours by using optogenetic feedback stimulation triggered upon the online detection of ripples in local field potentials (LFPs) recorded from the hippocampal CA1 region (Fig. 1A) (*15*). Simultaneous LFP recordings and electromyograms revealed that 84.6 ± 2.9% of the SW periods over 7 hours coincided with SW sleep, whereas the remaining SW periods were detected during awake immobility or consummatory behavior. Feedback illumination but not time-mismatched control illumination with random delays ranging from 80 to 120 ms to the dorsal CA3 region of somatostatin (SOM)::channelrhodopsin2 (ChR2) transgenic mice (Fig. 1B) reduced both ripple power (Fig. 1C) and the firing rates of CA1 pyramidal cells during the SWRs (Fig. 1C). This closed-loop technique silenced 97.7 ± 1.8% of the total SWRs (mean ± SEM of 10 trials from five mice). We measured field excitatory postsynaptic potentials (fEPSPs) from the CA1 stratum radiatum while single-pulse field stimulation was applied every 20 s to the Schaffer collaterals, which per se did not induce SWRs. Consistent with previous studies (*1*), the fEPSP slopes in no-light control and delayed control groups gradually decreased during the SW periods, but this spontaneous synaptic depression did not occur in the SWR-silenced mice (Fig. 1D). Neither the total sleep length nor the percentage occupied by each brain state differed between the groups (fig. S2), but the event incidence of SWRs remained higher in the SWR-silenced group (fig. S3).

After the SWRs were silenced for 7 hours, animals were tested in an object-place recognition task that consisted of two phases (Fig. 1E). During the first encoding phase, mice explored a familiar open arena with two identical novel objects, and none of the mouse groups exhibited a preference for one object over the other (fig. S4). The second recall phase, in which one of the objects was moved to a previously empty location, was conducted after a 2-hour resting period in the home cages. In this phase, the SWR-silenced group did not discriminate between the relocated and unmoved objects (Fig. 1F). Thus, object-place learning was disturbed after SWR silencing during SW states.

To more directly examine whether SWRs induce synaptic depression, we used obliquely sliced hippocampal preparations (*16*), which spontaneously emit SWRs (fig. S5). Slices prepared from animals that had explored a novel environment for 30 min exhibited higher SWR event frequencies than slices from naïve mice (fig. S5). Therefore, in the following experiments, we used slices from animals after exploration. Single-pulse field stimulation was applied to the Schaffer collaterals, and fEPSPs were recorded from the CA1 stratum radiatum. The fEPSP slopes were spontaneously reduced over time, and this reduction was inhibited by bath application of 50 μM D-AP5, an *N*-methyl-D-aspartate receptor (NMDAR) antagonist (fig. S6A). Thus, the spontaneous depression reflected actively occurring synaptic plasticity (*17*) rather than deterioration of the slice preparations or synaptic fatigue. We also prepared conventional horizontal hippocampal slices, which do not emit SWRs (*16*). Although these slices did not exhibit spontaneous synaptic depression (fig. S6B), even without SWRs, synaptic depression was inducible in a D-AP5–sensitive manner when the Schaffer collaterals were repetitively stimulated at event timings of the SWRs recorded in vivo after spatial exploration but not under naïve conditions without exploration (fig. S7).

We used slices prepared from SOM::ChR2 mice to conduct closed-loop SWR inhibition (Fig. 2A). Blue light pulsed upon SWR detection suppressed the firing rates of the neurons during SWRs (Fig. 2B). The SWR silencing prevented spontaneous synaptic depression, whereas control stimulation with a delay of 100 ms failed to replicate this effect (Fig. 2C).

We next attempted to confirm the spontaneous synaptic depression in SWR-emitting slices at the single-synapse level. The head sizes of dendritic spines are correlated with synaptic strength (*18*, *19*) and are subject to shrinkage during NMDAR-dependent long-term depression (*20*). We therefore examined whether spine shrinkage accompanied the spontaneous synaptic depression. We prepared oblique hippocampal slices from Thy1-mGFP mice and performed two-photon imaging of spines on the apical dendrites of CA1 pyramidal cells for 180 min (fig. S8A). The mean head volume of the spines decreased spontaneously as a function of time, an effect that was blocked by 50 μM D-AP5 (fig. S8B). The mean density of the spines did not change, indicating that few spines disappeared during the recording time ($P = 0.686$, $U = 6.00$, Mann-Whitney *U* rank sum test). As spines are typically categorized into thin, stubby, and mushroom types, we separately analyzed spine shrinkage for these types (fig. S8C, left). Thin and stubby spines shrank in a D-AP5–sensitive manner, but mushroom spines maintained their volumes throughout our observation period (fig. S8C, right).

Given the heterogeneity and specificity in spine shrinkage, we reasoned that patterns of CA1 neuronal activity may also be modulated in an NMDAR-dependent manner, because individual synaptic weights collectively orchestrate patterns of neuronal activity (*21*). Arc-dVenus transgenic mice (*22*) were allowed to freely explore a

[1]Laboratory of Chemical Pharmacology, Graduate School of Pharmaceutical Sciences, The University of Tokyo, Tokyo, Japan. [2]Laboratory for Systems Neurophysiology, RIKEN Brain Science Institute, 2-1 Hirosawa, Wako City, Saitama, Japan. [3]Department of Morphological Brain Science, Graduate School of Medicine, Kyoto University, Kyoto, Japan. [4]Department of Cell Biology and Neuroscience, Juntendo University Graduate School of Medicine, Tokyo, Japan. [5]Center for Information and Neural Networks, National Institute of Information and Communications Technology, Osaka, Japan.
*These authors contributed equally to this work.
†Corresponding author. Email: yuji@ikegaya.jp (Y.I.); fujisawa@brain.riken.jp (S.F.)

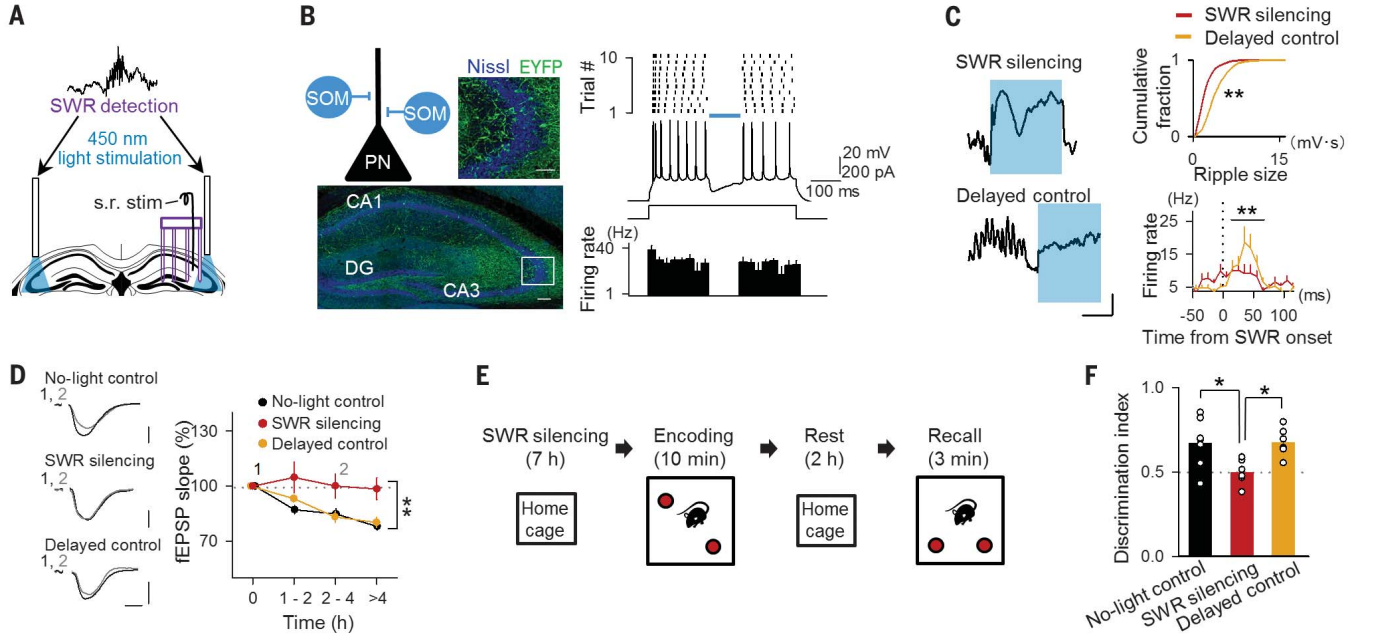

Fig. 1. SWR silencing prevents spontaneous synaptic depression during SW states and impairs subsequent spatial memory acquisition. (**A**) Schematic illustration of closed-loop SWR silencing. CA1 ripples were detected in real time after the experimental onset, triggering blue-light illumination targeting the bilateral dorsal CA3 region. s.r. stim, stratum radiatum stimulation. (**B**) (Left) Representative confocal image showing SOM::ChR2–enhanced yellow fluorescent protein (EYFP) expression in a hippocampal section that was counterstained with fluorescent Nissl. The boxed region is magnified in the top right image. Scale bars, 100 μm (top right) and 50 μm (bottom). DG, dentate gyrus. The top left image illustrates inhibition of a pyramidal neuron (PN) by SOM-positive interneurons. (Right) Whole-cell patch clamp recording showing that blue-light illumination suppressed current injection-evoked spiking in pyramidal cells. n = 5 cells in five slices from three mice. (**C**) (Left) Examples of the online feedback illumination (top) and control illumination with a delay (bottom). Scale bars, 0.2 mV (vertical) and 50 ms (horizontal). (Right) SWR silencing via SOM activation suppressed the ripple size (top) and SWR-locked units (bottom) recorded from CA1 shanks. Delayed illumination was used as a control. Kolmogorov-Smirnov test: $^{**}P = 2.7 \times 10^{-154}$, $D_{3693} = 0.437$, n = 1731 (silencing) and 1962 (delayed) ripples from six mice each. Mann-Whitney U rank sum test: $P = 1.0 \times 10^{-3}$, $U = 3477.0$, n = 18 (silencing) and 21 (delayed) cells from six mice. (**D**) Time course of the fEPSP slopes normalized at 0 min. SWR silencing during SW states suppressed the spontaneous fEPSP attenuation that occurred in the control groups. The images at left show typical fEPSP traces at times 1 and 2. Scale bars, 2 mV (vertical) and 5 ms (horizontal). Two-way analysis of variance (ANOVA), n = 6 mice each: $^{**}P = 5.5 \times 10^{-4}$, $F_{1,28} = 15.19$ versus no-light control; $^{**}P = 1.2 \times 10^{-3}$, $F_{1,30} = 12.90$ versus delayed control. (**E**) Behavioral paradigm. After SWR silencing in a home cage for 7 hours, mice were exposed to two identical objects for 10 min (encoding phase). After a 2-hour rest in the home cage, the mice were allowed to explore the same arena for 3 min with one of the objects relocated to the opposite corner (recall phase). The preferential exploration of the relocated object was measured as memory recall. (**F**) Discrimination indices during the recall phase were computed during the first 3 min of exploration. The SWR-silenced mice did not discriminate between the objects. Tukey's test after one-way ANOVA, n = 6 or 7 mice: $^{*}P = 0.031$, $Q_{3,16} = 4.00$ versus no-light control; $^{*}P = 0.033$, $Q_{3,16} = 3.96$ versus delayed control.

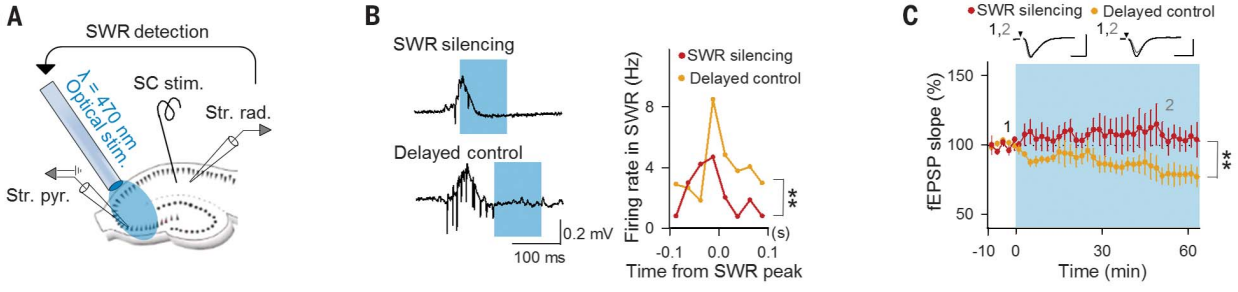

Fig. 2. Inhibiting hippocampal neurons during SWR impairs spontaneous synaptic depression in SWR-emitting slices. (**A**) Experimental procedures for recording fEPSPs at CA3 and CA1 synapses and silencing SWRs. SWRs and fEPSPs in the CA1 region were monitored in hippocampal slices prepared from SOM::ChR2-EYFP transgenic mice. A stimulating electrode was placed on the CA1 stratum radiatum to stimulate Schaffer collateral (SC) afferents. As SWRs were detected online, blue-light pulses were applied through an objective lens located over the CA3 region. Str. rad., stratum radiatum; Str. pyr., stratum pyramidale. (**B**) (Left) Examples of online feedback illumination (top) and control illumination with a delay of 100 ms (bottom). Cyan boxes indicate the periods of light illumination. (Right) SOM activation during SWRs, but not outside of SWRs, suppressed SWR-locked multiunits. Z test for comparing two counts, n = 3197 and 863 events: $^{**}P = 4.0 \times 10^{-13}$. (**C**) Time course of the fEPSP slopes after closed-loop illumination. SWR silencing but not delayed control impaired the spontaneous fEPSP depression. The slopes were normalized to the 10-min baseline values. The insets show typical fEPSP traces at times 1 and 2. Scale bars, 0.3 mV (vertical) and 20 ms (horizontal). Two-way ANOVA, n = 5 slices: $^{**}P = 3.1 \times 10^{-15}$, $F_{1,237} = 71.3$.

novel environment for 30 min (Fig. 3A) and were euthanized for hippocampal slice preparations. Cells positive for the modified yellow fluorescent protein dVenus (dVenus$^+$) putatively corresponded to neurons that had been activated during the exploration of the novel environment (*16*). We monitored the activity of CA1 neurons by functional calcium imaging while recording CA1 LFPs (Fig. 3B). Although dVenus$^+$ and dVenus$^-$ neurons were both activated during SWRs, dVenus$^+$ neurons tended to be more likely to participate in SWRs than dVenus$^-$ neurons (Fig. 3C). After 40 min, this difference increased further; that is, the SWR participation probability (the mean probability that a given cell exhibited a calcium transient during a given SWR event) became significantly higher for dVenus$^+$ cells than for dVenus$^-$ cells, mainly through a decrease in the probability of the SWR participation probability in dVenus$^-$ cells (Fig. 3D). The participation probability of neither dVenus$^+$ nor dVenus$^-$ cells was altered by treatment of slices with D-AP5 (Fig. 3E). Thus, the proportion of dVenus$^+$ cells in the cells activated during SWRs increased over time.

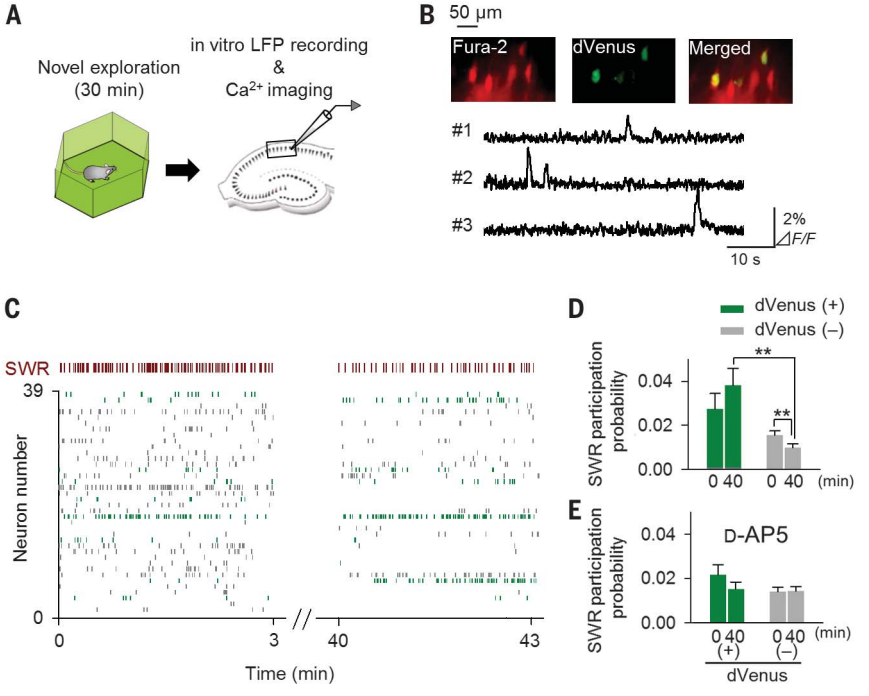

Fig. 3. NMDAR regulates the refinement of in vitro engram reactivation. (**A**) Experimental procedures for the in vitro SWR assay using hippocampal slices prepared from Arc-dVenus mice that had explored a novel environment for 30 min. (**B**) (Top) Calcium imaging from dVenus$^+$ and dVenus$^-$ CA1 neurons loaded with Fura-2AM. (Bottom) Three representative traces of the Fura-2AM–loaded neurons. *F*, fluorescence. (**C**) Representative raster plot of 39 simultaneously recorded CA1 cells around 0 and 40 min. The first set of images was taken 5 min after the SWR event frequency reached 0.80 Hz (see materials and methods for details). (**D**) The participation probability of dVenus$^-$ neurons during SWRs (participation rates) was smaller at 40 min than at 0 min, whereas the participation probability of dVenus$^+$ neurons did not change over time. dVenus$^-$ at 0 min versus dVenus$^-$ at 40 min: $^{**}P = 8.0 \times 10^{-5}$, $U = 15{,}991$; dVenus$^+$ at 40 min versus dVenus$^-$ at 40 min: $^{**}P = 3.2 \times 10^{-5}$, $U = 1960$; Mann-Whitney *U* rank sum test with Bonferroni's correction. Error bars indicate SEM of 192 dVenus$^-$ and 31 dVenus$^+$ cells. (**E**) The participation probability of neither dVenus$^+$ nor dVenus$^-$ neurons in slices treated with 50 μM D-AP5 differed between 0 and 40 min. dVenus$^+$: $P = 0.47$, $U = 488.5$; dVenus$^-$: $P = 0.34$, $U = 10{,}571$. Error bars indicate SEM of 39 dVenus$^-$ and 145 dVenus$^+$ cells.

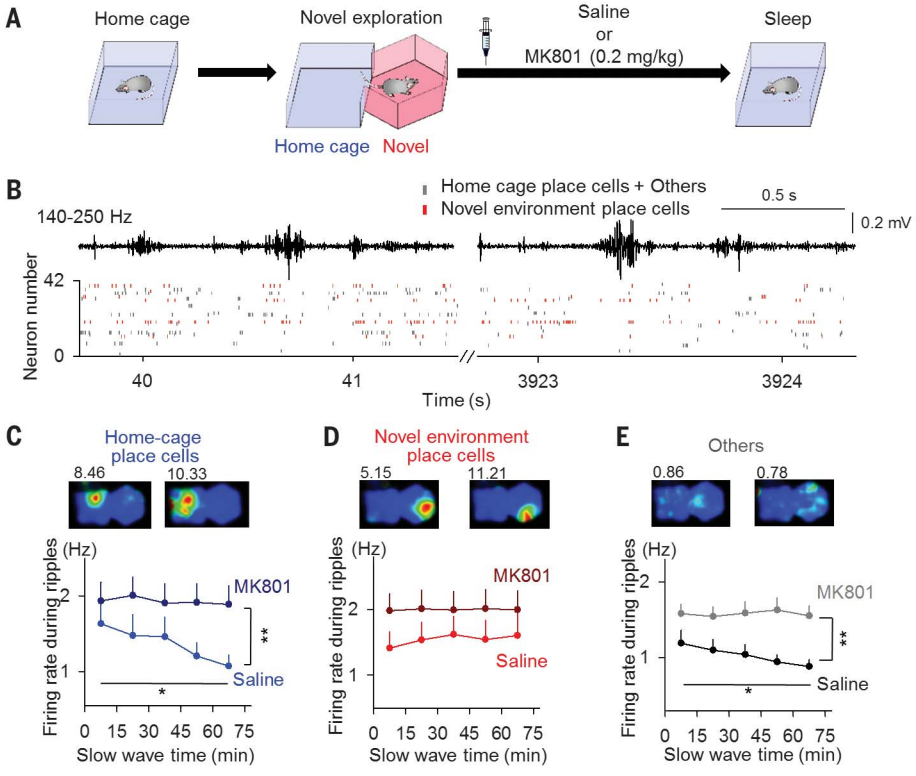

Fig. 4. NMDAR regulates the refinement of memory reactivation. (**A**) Time course of the experimental procedures. (**B**) Examples of representative spike events in a sleep session. The red rectangles indicate spikes of neurons that had place fields in the novel environment. The top traces represent ripple-band LFPs. (**C** to **E**) (Top) Color-coded rate maps for neurons with place fields in the home cage (C) and novel environment (D) and for other nonplace cells (E). The numbers above the maps represent the peak firing rates (hertz). (Bottom) Time courses of firing rates in SWRs during SW periods. SWR-relevant firing rates of home-cage place cells and other cells, but not novel-environment place cells, decreased with time, an effect that was abolished by the systemic injection of MK801. Home-cage place cells: $^{*}P = 0.048$, $Z = -5.88$; others: $^{*}P = 0.026$, $Z = -1.95$; Jonckheere-Terpstra trend test. Home-cage place cells: $P = 7.3 \times 10^{-4}$, $F_{1,368} = 11.6$; others: $P = 8.5 \times 10^{-4}$, $F_{1,1470} = 11.1$; two-way ANOVA. $n = 37$ to 145 cells from eight or nine trials from three mice (saline) and 28 to 195 cells from eight or nine trials from three mice (MK801).

Finally, we examined whether an NMDAR-dependent refinement of neuronal activity during SWRs also occurs in vivo. Mice were implanted with 32-site silicon probes in the CA1 region to monitor LFPs and unit spikes while the mice traversed their home cages. Each home cage was immediately joined to a novel environment that was not accessible to the mice unless an experiment was being conducted. During the 30-min exploration period in the novel environment, new place cells were detected in addition to the pre-established place cells in the home cage. Immediately after the exploration, the mice were treated intraperitoneally with either saline or 0.2 mg of MK801, an NMDAR blocker, per kilogram of body weight (Fig. 4A). Then, the mice were placed in the original home cage for 4 to 6 hours, and spikes during SW states were analyzed. The place cells were reactivated during SWRs (Fig. 4B). In the saline group, the novel-environment place cells did not change their firing rates during the SWRs throughout the entire recording session, whereas the home-cage place cells and the other cells that did not code either place in the environment (others) gradually decreased their SWR-related firing rates (Fig. 4, C to E). In the MK801-treated group, neither neuron type exhibited such delays in the firing rates (Fig. 4, C to E).

We discovered that hippocampal SWRs triggered persistent synaptic depression and that silencing SWRs impaired subsequent new learning, which appears to be consistent with the hypothesis that overstrengthened synapses impair neuronal responsiveness and saturate the ability to learn (*23*, *24*). We consider three possible but not mutually exclusive mechanisms by which SWRs induce synaptic depression: (i) synaptic delay lines in activity propagation during SWRs decouple hippocampal network activity and weaken synaptic weights (*10*), (ii) uncorrelated presynaptic and postsynaptic activity during SWRs causes heterosynaptic depression because memory-irrelevant cells are rarely fired during SWRs (*25*), and (iii) the event frequency of SWRs reaches ~1 Hz after spatial exploration, which may induce homosynaptic depression (*26*, *27*). Notably, field stimulation with the event timing of SWRs after spatial exploration was sufficient to induce depression, suggesting the importance of the role of the timing, rather than the spike contents, of SWRs. On the other hand, mushroom spines did not shrink in SWR-emitting slices; that is, not all spines were equally subject to depression. This finding is in agreement with the hypothesis that sleep leads to net depression through the removal of unstable synapses [(*28*), but see also (*29*)]. A recent in vitro study demonstrated that the relative spike timings of CA3 and CA1 place cells during SWRs cause synaptic potentiation (*9*). Thus, synapses involved in memory engrams may escape depression through presynaptic and postsynaptic coactivation. Together with our findings, we propose dual roles of SWR-induced depression: (i) SWRs reset unnecessary synapses and avoid memory saturation (*30*), and (ii) SWRs purify recent memory engrams by shearing irrelevant neuronal activity and perhaps strengthening memory-relevant synapses, thereby contributing to memory consolidation.

REFERENCES AND NOTES

1. V. V. Vyazovskiy, C. Cirelli, M. Pfister-Genskow, U. Faraguna, G. Tononi, *Nat. Neurosci.* **11**, 200–208 (2008).
2. R. Huber *et al.*, *Cereb. Cortex* **23**, 332–338 (2013).
3. G. Tononi, C. Cirelli, *Brain Res. Bull.* **62**, 143–150 (2003).
4. G. Tononi, C. Cirelli, *Neuron* **81**, 12–34 (2014).
5. A. K. Lee, M. A. Wilson, *Neuron* **36**, 1183–1194 (2002).
6. V. Ego-Stengel, M. A. Wilson, *Hippocampus* **20**, 1–10 (2010).
7. G. Girardeau, K. Benchenane, S. I. Wiener, G. Buzsáki, M. B. Zugaro, *Nat. Neurosci.* **12**, 1222–1223 (2009).
8. G. M. van de Ven, S. Trouche, C. G. McNamara, K. Allen, D. Dupret, *Neuron* **92**, 968–974 (2016).
9. J. H. Sadowski, M. W. Jones, J. R. Mellor, *Cell Rep.* **14**, 1916–1929 (2016).
10. E. V. Lubenov, A. G. Siapas, *Neuron* **58**, 118–131 (2008).
11. L. L. Colgin, D. Kubota, Y. Jia, C. S. Rex, G. Lynch, *J. Physiol.* **558**, 953–961 (2004).
12. O. Bukalo, E. Campanac, D. A. Hoffman, R. D. Fields, *Proc. Natl. Acad. Sci. U.S.A.* **110**, 5175–5180 (2013).
13. O. Eschenko, W. Ramadan, M. Mölle, J. Born, S. J. Sara, *Learn. Mem.* **15**, 222–228 (2008).
14. C. J. Behrens, L. P. van den Boom, L. de Hoz, A. Friedman, U. Heinemann, *Nat. Neurosci.* **8**, 1560–1567 (2005).
15. E. Stark *et al.*, *Neuron* **83**, 467–480 (2014).
16. M. Mizunuma *et al.*, *Nat. Neurosci.* **17**, 503–505 (2014).
17. G. L. Collingridge, S. J. Kehl, H. McLennan, *J. Physiol.* **334**, 33–46 (1983).
18. M. Matsuzaki *et al.*, *Nat. Neurosci.* **4**, 1086–1092 (2001).
19. M. Masugi-Tokita *et al.*, *J. Neurosci.* **27**, 2135–2144 (2007).
20. Q. Zhou, K. J. Homma, M. M. Poo, *Neuron* **44**, 749–757 (2004).
21. O. Paulsen, T. J. Sejnowski, *Curr. Opin. Neurobiol.* **10**, 172–179 (2000).
22. M. Eguchi, S. Yamaguchi, *Neuroimage* **44**, 1274–1283 (2009).
23. D. Balduzzi, G. Tononi, *Theory Biosci.* **132**, 27–39 (2013).
24. S. S. Yoo *et al.*, *Nat. Neurosci.* **10**, 385–392 (2007).
25. G. S. Lynch, T. Dunwiddie, V. Gribkoff, *Nature* **266**, 737–739 (1977).
26. R. M. Mulkey, R. C. Malenka, *Neuron* **9**, 967–975 (1992).
27. S. M. Dudek, M. F. Bear, *Proc. Natl. Acad. Sci. U.S.A.* **89**, 4363–4367 (1992).
28. L. de Vivo *et al.*, *Science* **355**, 507–510 (2017).
29. G. H. Diering *et al.*, *Science* **355**, 511–515 (2017).
30. M. R. Mehta, *Nat. Neurosci.* **10**, 13–15 (2007).

ACKNOWLEDGMENTS

We thank C. Cirelli, L. Fenk, Y. Goda, G. Laurent, T. McHugh, S. Reiter, and G. Tononi for comments on early versions of the manuscript; T. Danjo and Y. K. Park for technical assistance; and S. Yamaguchi for providing Arc-dVenus mice. **Funding:** This work was supported by Ministry of Education, Culture, Sports, Science and Technology Grants-in-Aid for Scientific Research (25119004 and 26250003 to Y.I. and 16H01519 to S.F.); "Resonance Bio" (16H01426 to H.H.); Japan Society for the Promotion of Science Grant-in-Aid for Research Activity start-up (16H07453 to H.N.); RIKEN Special Postdoctoral Researchers Program research grant (201600059347 to H.N.); the Sasakawa Scientific Research Grant from the Japan Science Society (28-402 to H.N.); Brain/MINDS (Brain Mapping by Integrated Neurotechnologies for Disease Studies) from the Japan Agency for Medical Research and Development (AMED) (to H.H. and S.F.); the Strategic Research Program for Brain Sciences on "Development of BMI Technologies for Clinical Application" (to Y.I.); and a Human Frontier Science Program (RGP0019/2016 to Y.I.). This work was partly facilitated by a program in the International Research Center for Neurointelligence (WPI-IRCN) of The University of Tokyo Institutes for Advanced Study at The University of Tokyo. **Author contributions:** H.N., S.F., and Y.I. designed and implemented the study and wrote the manuscript. H.N., Y.S., and S.F. performed in vivo physiology. K.M. performed immunohistochemistry. H.N., M.G., and K.O. performed in vitro electrophysiology. H.N. and T.I. performed optical recording. T.S. and H.H. helped with analysis. All authors discussed the results and commented on the manuscript. **Competing interests:** The authors declare no competing interests. **Data and materials availability:** All data necessary to support this paper's conclusions are available in the main paper or the supplementary materials. The full primary data are available at http://ikegaya.jp/data/norimoto_science2018/.

SUPPLEMENTARY MATERIALS

www.sciencemag.org/content/359/6383/1524/suppl/DC1
Materials and Methods
Figs. S1 to S8
References (*31*–*42*)

10 June 2017; accepted 26 January 2018
Published online 8 February 2018
10.1126/science.aao0702

Hippocampal ripples down-regulate synapses

Hiroaki Norimoto, Kenichi Makino, Mengxuan Gao, Yu Shikano, Kazuki Okamoto, Tomoe Ishikawa, Takuya Sasaki, Hiroyuki Hioki, Shigeyoshi Fujisawa and Yuji Ikegaya

Science **359** (6383), 1524-1527.
DOI: 10.1126/science.aao0702originally published online February 8, 2018

Rebalancing mechanisms during sleep

Synapses are often strengthened during wake periods and thus need to be homeostatically readjusted during sleep. During slow-wave sleep, synaptic depression is dominant. Sharp wave and ripple events are transient high-frequency field oscillations that occur spontaneously during slow-wave sleep in the brain. Norimoto *et al.* found that these events induced long-term depression of hippocampal synapses and may thus help to refine recently acquired memories (see the Perspective by Draguhn).

Science, this issue p. 1524; see also p. 1461